Available online at www.sciencedirect.com
SCIENCE DIRECT®
International Journal of Heat and Mass Transfer 47 (2004) 2587–2598
International Journal of HEAT and MASS TRANSFER
www.elsevier.com/locate/ijhmt

Wave-augmented mass transfer in a liquid film falling inside a vertical tube

C.D. Park [a], T. Nosoko [a,*], S. Gima [a], S.T. Ro [b]

[a] Department of Mechanical and Systems Engineering, University of the Ryukyus, Nishihara, Okinawa 903-0213, Japan
[b] Department of Mechanical Engineering, Seoul National University, San 56-1, Shilim-dong, Kwanak-gu, Seoul 151-742, South Korea

Received 31 July 2003; received in revised form 19 December 2003

Abstract

Uniformly distributed water films were formed inside vertical tubes, and partial disintegrations of hump-like surface waves (or large waves) into clusters of dimples were observed on the films at the Reynolds number $Re \sim 40$ and larger, associated with marked deceleration of mass-transfer augmentation. In about 1 m or taller films with the uniform distribution, two empirical correlations between the Sherwood number Sh and Re at the ranges of $Re = 20$–40 and 40–400 were constructed. The transition to turbulent flow occurs in the films with decelerating inlet flow at the range of $Re = 400$–700 where Sh sharply rises, suggesting that the laminar developing entry region rapidly shortens to nearly disappear, though the region had been observed only in film flow measurements. Periodic perturbations imposed on the inlet flow trigger tall humps close to the inlet, causing the laminar developing region to vanish and the critical Re to reduce from 400 to about 300. Waves covering a whole film of 0.4–1.0 m height increase in Sh up to 2.2–2.7 times the theoretical prediction for a smooth film at the laminar-flow range. The amount of increase is larger in a taller film. The decrease in Sh due to the tube inclination from the vertical is more serious for a taller film with laminar flow, and a 0.2° inclination causes a 5% decrease in a 0.7 m tall film.

Keywords: Falling film; Surface wave; Mass transfer; Flow transition; Turbulent flow; Laminar entry region

1. Introduction

Falling liquid films are widely utilized in industry for interfacial heat/mass transfer processes in gas absorbers, chemical reactors, evaporators, condensers, cooling towers, etc. Wave-induced convections are most intense at or near the film surface, and thus they drastically augment the mass transfer from the surface into the bulk of film and vice versa; otherwise the mass transfer rate is very small due to the low molecular diffusion. Several researchers measured the mean mass transfer coefficient k_L in films falling down vertical walls at various flow rates as reviewed by Alekseenko et al. [1], Roberts and Chang [2], Bakopoulos [3], Hikita et al. [4] and Kamei and Oishi [5]. These measurements show that the mean mass transfer coefficient k_L rapidly increases at small Re, after which the rate of increase suddenly drops at a certain Re and then continue to increase slowly until the turbulent-flow range of Re is reached whereby the coefficient starts to sharply increase again. The critical Reynolds numbers seem to be in 40–75 and 300–400 for the first and second transitions, respectively, though the measurements scatter widely. In the laminar flow range surface waves may augment the coefficient k_L of 0.3–0.65 and 1.1–2.5 m tall films up to 2–3 and 2.5–5.5 times the prediction for a flat film, respectively [2]. For practical use, Bakopoulos [3] constructed empirical correlations of the Sherwood number Sh as a function of Re at the three Re ranges for water films. He selected the measurements of Kamei and Oishi [5], Hikita et al. [4], Lamourelle and Sandall [6] and Emmert and Pigford [7] where most of the data had been determined in 1 m or

* Corresponding author. Tel./fax: +81-98-895-8616.
E-mail address: yongrang@tec.u-ryukyu.ac.jp (T. Nosoko).

0017-9310/$ - see front matter © 2004 Elsevier Ltd. All rights reserved.
doi:10.1016/j.ijheatmasstransfer.2003.12.017

Nomenclature

C	dissolved oxygen concentration, g/m^3
D	mass diffusivity, m^2/s
f	frequency of periodic inlet perturbation, 1/s
g	gravitational acceleration, m/s^2
k_L	mean mass transfer coefficient, m/s
L_{sm}	length of smooth entry pass, m
L_f	film height, m
Q	volumetric flow rate, m^3/s
R	inner radius of tube, m
Re	Reynolds number, $Q/(2\pi Rv)$
Sc	Schmidt number, v/D
Sh	Sherwood number, $(k_L\delta)/D$
x	downstream distance from the film inlet, m

Greek symbols

δ	mean film thickness, m
v	kinematic viscosity, m^2/s
θ	tube inclination from vertical, deg

Subscripts

fc	forced wave
in	film entry
N	Nusselt film
nt	naturally formed wave
out	film exit
s	saturated

taller films, so that his correlations can neglect the effect of the film height or the smooth entry pass. Waves appear at some downstream distance on the entry smooth surface, and the length of the smooth entry pass increases with Re up to about 0.3 m [8].

The dynamics of surface waves varies with both the flow rate and the downstream distance x [9–15]. Waves appear on the smooth surface and soon coalesce to develop into teardrop-shaped tall waves (or humps) traveling on a thin substrate at high speeds [16]. The consequent humps (often referred to as 'large waves' [17]) intermittently coalesce to further develop into taller humps with large separations [18–20]. Such process of integrating waves into lesser numbers of taller humps is observed at wide Re ranges of both laminar and turbulent flow, and the wave integration process seems to be rapid to distances of about 0.5 m from the film inlet and then become slow further downstream. Takahama and Kato [13] measured film-thickness variations at various downstream distances and showed that the amplitude of humps and the standard deviation of film-thickness variation rapidly increase in about 0.5 m long entry zone. Humps out of the entry zone have a nearly constant dimensionless speed of about 1.3 with respect to the mean velocity in the film, and gradually increase the mean separation between humps. Such slow integration process continues to $x \sim 2.5$ m or further downstream at $Re \sim 170$ and larger, associated with a gradual increase in the standard deviation of film thickness [15]. The wave dynamics might reach the final saturation at $x \sim 6$ m or further downstream [12].

The humps undergo not only the wave integration but also partial disintegration. Recently Park and Nosoko [16] revealed that humps disintegrate into several horseshoe-shaped humps at $Re \sim 40$ or larger, causing the first transition of the mass transfer, and the partial disintegration become more intense at larger Re associated with the marked deceleration of the mass transfer augmentation.

For the film flow, the structure of turbulent flow and the transition to turbulent flow have not been fully understood in spite of numerous studies on falling films. The film flow is *wavy-laminar* in the laminar-flow range, and the transition to turbulent flow seems to occur in a manner different from that observed in wall boundary shear layers. Karimi and Kawaji [21,22] detected *localized* turbulent flow under waves with large fluctuations of film-surface height. From the breaks in curves of the local mean film thickness vs. Re, Takahama and Kato [13] detected the transition to turbulent flow, and derived the conclusion that a film has a wavy-laminar entry region preceding to the transition to turbulent flow and this laminar developing entry region gradually retracts upstream from $x \sim 1.3$ to $\sim$0.9 m with Re increasing from 370 to 750 and then rapidly diminishes to be close to the inlet at $Re \sim 800$ or larger. Brauer's [11], Feind's [23] and Wilke's [24] experiments may support Takahama and Kato's findings, and suggest the transition range from $Re \sim 400$ to 800; At this Re range, the wave peak height become constant [11], the mean heat transfer coefficient from tube wall to film has the largest slope of the coefficient–Re curve on log–log graph [24], and the mean film-thickness curves have breaks within the Re range for liquids of various viscosities and surface tensions. One may expect that such behavior of the laminar developing entry region brings about drastic changes in the mass transfer between the surface and the bulk at the transition range of Re.

In the present work, we determined the mean mass transfer coefficient k_L for films discharged uniformly through the newly designed feeding device (see Fig. 1) that greatly improves the uniform distribution of liquid along a tube inner circumference. A slight variation of the distribution causes a serious reduction in the mass

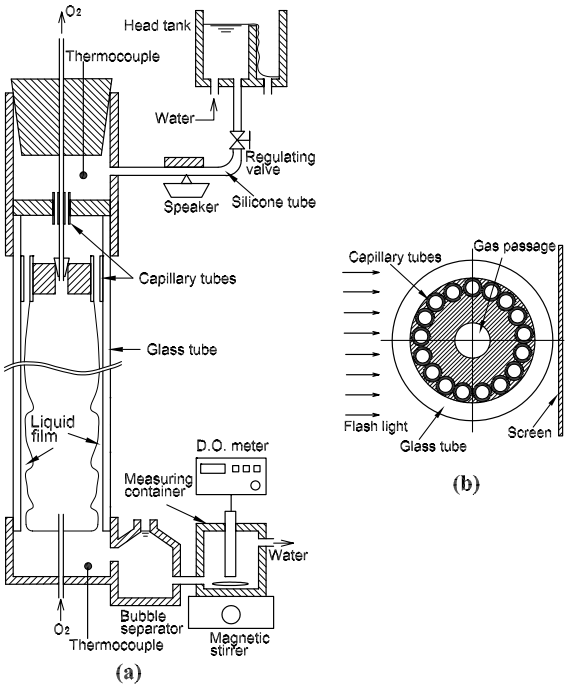

Fig. 1. Experimental apparatus: (a) flow diagram of water and oxygen gas and (b) cross-section of distributor consisting of capillary tubes, and arrangement of screen, glass tube and light rays.

transfer rate. The new design is an updated version of the 'undulated annular distributor' designed by Brauer and Thiele [25], in which liquid is discharged into a film through several channels arranged along the circumference. Though in most of engineering applications and experimental studies, falling films have been formed on tube walls by liquid flowing over a weir or through ring slots [3,26], both methods have serious difficulties in obtaining uniform distribution, especially at low flow rates. According to Bakopoulos [3] and our preliminary experiments, diminutive variations in the slot width and in liquid velocity entering the slot may ruin the uniform distribution, and for the overflowing, diminutive manufacturing defects of the tube top edge, flow disturbances in liquid pool around the tube edge and imperfection of vertical tube alignment.

With the uniformly distributed films, we explored the mass transfer in the transition range from the wavy-laminar to turbulent flow, as well as the effect of the smooth entry pass on the mass transfer at the laminar-flow range, by imposing perturbations of a low constant frequency on the inlet film flow. Such inlet forcings may greatly shorten both the laminar developing entry region preceding the transition to turbulent flow and the smooth entry pass preceding the wavy-laminar flow. The initial evolution of the wave is extremely sensitive to disturbances included in the inlet flow, and the *naturally* formed waves, which have been investigated by many researchers, are noise-driven and have frequencies within a narrow band at their inception [18,27]. Then the waves (or humps) increase the separations through coalescence events as they travel downstream. When the inlet forcings are adequately larger in amplitude than the noise included in the inlet flow, waves at the corresponding low frequency appear close to the inlet, and then directly grow into tall humps with large separations. Comparisons in the mass transfer between the forced waves and the natural waves may allow one to determine the variation of the laminar developing entry region in the transition range of Re, as well as the effect of the smooth entry pass on the mass transfer at the laminar-flow range. Furthermore, we examined the effect of the tube inclination θ from the vertical, which may be important when installing equipment in practical applications. Liquid uniformly discharged at the inlet may gradually accumulate as it flows downstream inside a slightly inclined tube, causing a reduction of the mass transfer rate. This tube inclination effect can be determined with uniform distribution.

2. Experimental apparatus and procedure

Tap water flows from a head tank through a silicone tube into a two-story holding compartment at the top of glass tube, and then the water is uniformly distributed through 17 capillary tubes arranged along the 9.6 mm inner tube wall to form a film (Fig. 1). Oxygen-rich water flows from the pool at the bottom of the tube through a bubble separator into a measuring container where the dissolved oxygen concentration C_{out} is measured with a galvanic cell within 1% error. Oxygen gas flows upwards through the tube core space and its flow rate is so low that both the pressure rise inside the tube as a result of the gas flow and the effect of the gas flow on the wave dynamics are negligible. A thin plate fixed to a speaker cone vibrates the silicone tube to impose periodic perturbations on the water flow. Power input into the speaker is adjusted to trigger large waves (or humps) to develop shortly downstream of the film inlet. A holder of the glass tube is fixed to a steel pole standing on a mechanical stage, which can change the tube inclination θ with 0.08° accuracy.

The capillary tubes are 15 mm long and 1.0 mm inner diameter (Fig. 1b), and differences in flow rate through each tube are very small (within ±2%). Jets from the tubes merge at the tube exits to form a film, and thus the inlet film flow includes transverse disturbances of a 1.4 mm wavelength, i.e. the interval between tubes. This transverse wavelength is much shorter than the most unstable wavelength of about 2 cm found by Park and Nosoko [16]. The average velocity in each tube exceeds

the average velocity in the smooth entry to the film (equal to the average velocity in Nusselt film) at $Re \sim 280$ or larger, showing that the flow decelerates in the entry at $Re \sim 280$ or larger. At large Re, the film drags along bubbles into the water pool at the bottom. The water flow from the pool brings about a circulation flow inside the bubble separator for the bubbles to accumulate in the center and float up to the water surface.

The water temperature was measured by the calibrated T-type thermocouples at the top and bottom of the tube within a ±0.1 K error, and the average of both readings, i.e. the film temperature, was 15–24 °C for the mass transfer measurements. The mass flow rate of water was measured at the exit of the container within a ±0.5% error. The oxygen concentration in tap water was measured before and after the experimental runs in a day, and the average of these two was assumed to be the inlet concentration C_{in}, though the differences between the two were less than 1% for most of the measurements.

Flashlight from a stroboscope passes through the glass tube and projects the shadows of the film on the screen (Fig. 1b). The shadow image is captured by a camera synchronized with the stroboscope. The flashlight passes through the annular film, and therefore two shadow images of front and back parts of the tube inner wall are projected, overlapping on the screen and the tube curvature distorts wave shadows. These may bring some difficulty when one observes the shadow images.

We employ the Reynolds number Re, the Schmidt number Sc and the Sherwood number Sh defined as,

$$Re = \frac{Q}{(2\pi R\nu)}, \quad Sc = \frac{\nu}{D}, \quad Sh = \frac{k_L\delta}{D} \tag{1–3}$$

where the mean film thickness δ is calculated from one of the following correlations,

$$\delta = \left(\frac{3\nu^2 Re}{g}\right)^{1/3} \quad \text{at } Re < 400,$$
$$\delta = 0.302\left(\frac{3\nu^2}{g}\right)^{1/3} Re^{8/15} \quad \text{at } Re > 400 \tag{4,5}$$

The first equation for δ is applicable to the fully developed flat film (referred to as Nusselt film) and *wavy-laminar* films, and the second, to turbulent-flow films [11].

The mean mass transfer coefficient k_L is calculated from

$$k_L = \frac{Q}{2\pi(R-\delta)L_f} \ln\frac{C_{\text{s}} - C_{\text{in}}}{C_{\text{s}} - C_{\text{out}}} \tag{6}$$

The saturated concentration C_{s} was calculated from Truesdale et al.'s [28] correlation with the film temperature and the partial pressure of oxygen at the film surface. The partial pressure was assumed to be the difference between the ambient pressure and the saturate pressure of water at the film temperature. An error in k_L or Sh arising from the measurements of C, Q and L_{f} is small, and diminutive imperfection of uniform distribution and excess absorption from bubbles pulled into the water dominate the overall error in Sh, which is roughly estimated to be ±4% at the laminar-flow range of Re from the scattering of the measurements and others. At the turbulent-flow range, the bubble separator could not remove the bubbles pulled into the water completely. Thus the measurements of Sh have positive deviations at the turbulent-flow range, and this is discussed in the proceeding section. The error in Re is found to be ±1% or less. The diffusivity D was calculated from Stokes–Einstein equation (refer to [16,30]), and the Schmidt number Sc was estimated to be 644–403 at the present working temperature of $T = 15$–24 °C.

3. Results and discussion

3.1. Wave dynamics

Teardrop-like waves (or humps) have deep valleys in their fronts and the front valleys form distinctive dark strips on the screen, which may represent their wavefronts [16,29,30]. Shadow images of surface waves are shown in Figs. 2 and 3 where several dark strips representing the wavefronts are marked by triangles with 'A' among many dark strips of wavefronts. At low Re, small waves appear on the smooth entry surface and then rapidly develop into teardrop-like tall humps (see Fig. 2a for $Re = 20.4$). Soon the humps coalesce to develop into taller humps (Fig. 2a for humps with longer separations at $x \sim 20$–30 cm in the shadow image of $Re = 20.4$), and then hump-coalescence events intermittently occur to generate further taller humps with much longer separations (Fig. 2a for humps at $x > 30$ cm in the shadow image of $Re = 20.4$). Humps increase the wavefront distortion and partially disintegrate into dimples at $Re \sim 40$ or larger (Fig. 2a for $Re = 89$) while the disintegration hardly occurs at smaller Re. One may identify such partial hump disintegrations from the resulting clusters of dimples (several clusters are marked by 'B' triangles among many clusters in Figs. 2 and 3) since strips for hump wavefronts are hardly observed when the strips and clusters of dark spots overlap on the images.

At high Re, the wave evolution is complex. Typically, isolated dimples first appear on the smooth entry surface, and then some of the dimples stretch out in the transverse direction to develop into teardrop-like humps with distorted wavefronts: the stretching dimples form the deep valleys in front of the humps (Fig. 2a for $Re = 200$). The resultant humps also partially disinte-

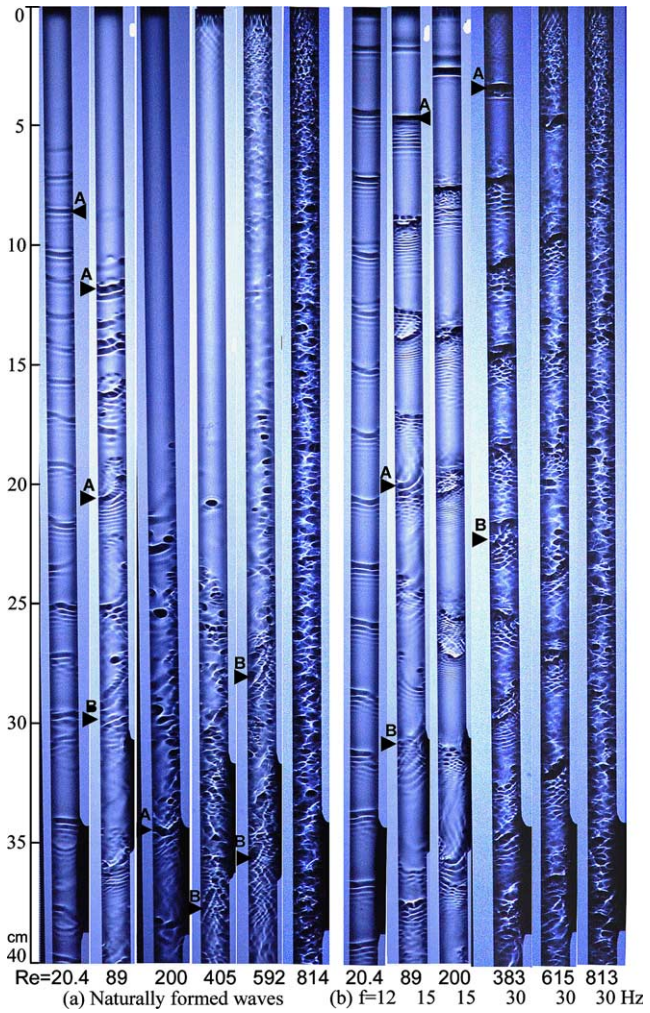

Fig. 2. Shadow images of smooth entry pass, humps and dimples at upstream region on a film at various *Re*: (a) naturally formed humps and dimples and (b) forced humps and their partial disintegration into dimples. Dark strips and spots represent hump wavefronts and dimples, respectively, and some humps are marked by triangles with A. At high *Re*, clusters of dimples may represents humps, and some of them are marked by triangles with B.

grate into clusters of dimples and split up, as they travel downwards.

The perturbations imposed on the inlet flow trigger humps with horizontal wavefronts to develop shortly downstream of the inlet at the corresponding frequency, resulting in the smooth entry pass to disappear (Fig. 2b). Then the humps increase the wavefront distortion to cause the partial disintegrations emitting dimples at $Re \sim 40$ or larger. Dimples spread on smooth substrates between humps at larger *Re*, and the whole film surface is covered with dimples at $Re \sim 700$ or larger, though these dimples are exaggerated on the overlapping shadow images.

As traveling downstream, both forced and natural humps intermittently coalesce to develop into a smaller number of larger humps with longer separations accompanying more dimples. The separation between humps increases to about 0.1 m far downstream through coalescence events (Fig. 3a). Such an increase in the hump separation was also captured by Takahama and Kato [13] on their local film-thickness measurements.

The smooth entry pass increases in length from about 5 cm at $Re \sim 20$ to the maximum of 20–35 cm at $Re \sim 400$, and then sharply decreases to disappear at $Re \sim 700$ or larger (Fig. 4). Here the wave inception line or point was determined on shadow images by the dark strip or dark spot appearing at the shortest distance x (Fig. 2a). At $400 < Re < 700$, the entry pass is fairly rough near the film inlet because of jets from the capillary tubes (Fig. 2a for $Re = 592$), and the wave inception

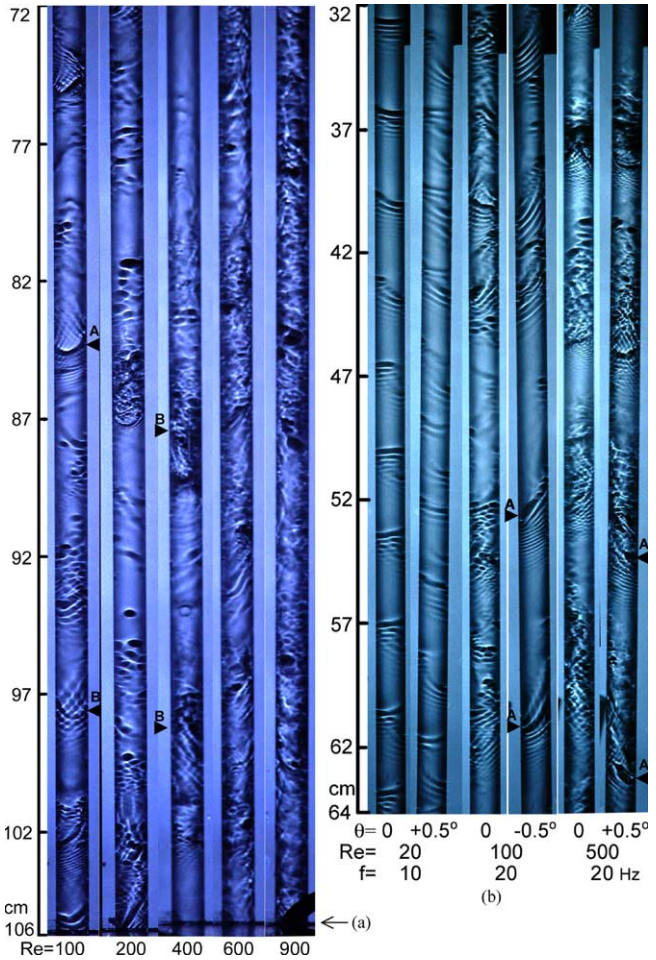

Fig. 3. Shadow images of humps and dimples at downstream and midstream regions: (a) naturally formed humps on a vertical film at $x = 0.72$–1.06 m and (b) forced humps on a vertical or inclined film at $x = 0.32$–0.64 m.

point was determined by a distinctly dark spot appearing first downstream of the rough surface. We assumed that the smooth entry pass is defined to be the area from the film inlet to the wave inception line or point. The inception of waves or dimples is very sensitive to the noise included in the inlet flow, and therefore the smooth entry length L_{sm} fluctuates largely. The present measurements are in good agreement with the observations made by Tailby and Portalski [8] and Stainthorp and Allen [31] at the laminar-flow range of $Re < 400$. They formed films of accelerating inlet flow by water flowing over a weir while in the films of the present work, it is estimated that the inlet flow from the capillary-tube distributor decelerates at $Re \sim 280$ or larger. This decelerating inlet flow causes a great change in the wave inception at the transition and turbulent-flow ranges of Re. Tailby and Portalski [8] observed that films with accelerating inlet flow further increase the smooth entry length to 0.31 m at $Re \sim 500$, and then level out. This difference is discussed in relation to its effect on the mass transfer in the latter section.

At small Re, natural waves at their inception have nearly horizontal wavefronts, and forced waves also have nearly horizontal wavefronts even far downstream (Fig. 2a and b for $Re = 20.4$). Our preliminary experiments showed that such horizontal wavefronts are hardly formed with diminutive defects in uniform distribution at small Re. These observations show that the superior uniform distribution was achieved with the new distributor employed.

3.2. Wave-augmented mass transfer and transition to turbulent flow

The Sherwood number Sh of a film about 1 m tall is proportional to Re raised to the power of 1.1, 0.5 and 1.25 at the ranges of $Re < 40$, $40 < Re < 400$ and $Re > 400$, respectively (Fig. 5a). The first break of the

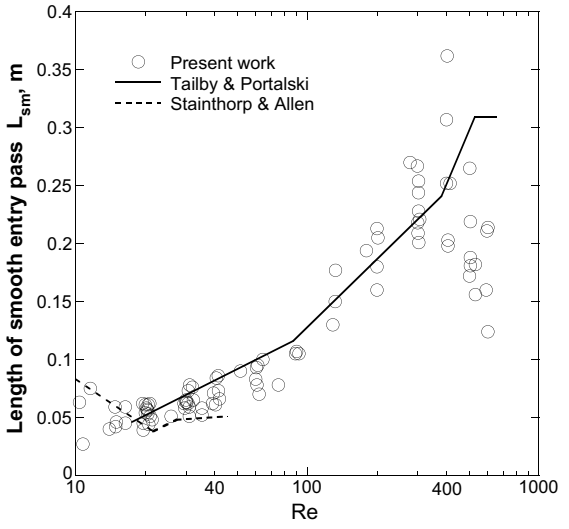

Fig. 4. Variation of length of smooth entry pass L_{sm} with Re.

Sh–Re curve at $Re \sim 40$ is caused by wavefront distortions associated with the partial wave disintegration into dimples. This observation is in agreement with Park and Nosoko's finding [16] that at $Re > 40$, humps increase the wavefront distortion to break the wavefronts into several horseshoe shapes associated with marked deceleration of the mass transfer enhancement. The transition to turbulent flow causes the second break at $Re \sim 400$, and this critical value was also determined by Brauer [11] and Feind [23] from measurements of the film thickness and the wall shear stress, respectively.

Bakopoulos' correlations [3] are in excellent agreement with the present measurements for the tall film with natural and forced waves at $Re = 70$–300. At $30 < Re < 70$, however, the present data are larger than his correlations. The present results suggest that for uniformly distributed films of about 1 m height or taller at $Re < 70$, Bakopoulos' correlations may have to be revised to, an extension of Bakopoulos' second correlation, $Sh = 8.0 \times 10^{-2} Re^{0.5} Sc^{0.5}$ from $Re > 70$ to $Re > 40$, and a new correlation, $Sh = 8.8 \times 10^{-3} Re^{1.1} Sc^{0.5}$ at $20 < Re < 40$ (see Fig. 5a).

The revised correlations pass through or near the upper boundary of Kamei and Oishi's [5] and Hikita et al.'s [4] measurements which supplied the main body of the data for Bakopoulos' first and second correlations, while his existing correlations pass through or near the lower boundary (refer to Fig. 1 in [3]). Kamei and Oishi [5] and Hikita et al. [4] formed films through *overflowing*, and Bakopoulos cited the serious difficulties in obtaining uniform distribution by overflowing especially at low flow rates. Bakopoulos' measurements of the mass transfer in a film discharged from an undulated annular distributor fall on or near the revised

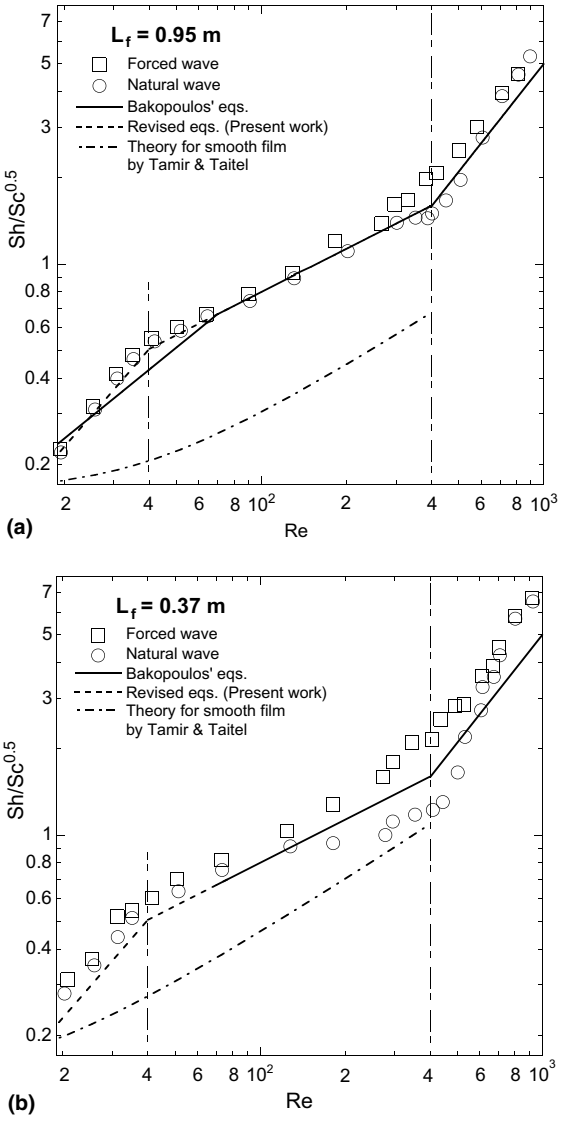

Fig. 5. Variation of *Sh* with *Re* for (a) 0.95 m and (b) 0.37 m tall films. Solutions by Tamir and Taitel [34] to the equation of diffusion in smooth film are presented for comparison, and Bakopoulos' correlations are revised to fit the plots for uniformly distributed film at $20 < Re < 40$ and $40 < Re < 70$.

correlations and are larger than those in film discharged from a ring slot (refer to Fig. 6 in [3]).

The measurements of *Sh* are larger by approximately 17% for forced waves on the short film of 0.37 m height than the 0.95 m tall film at both ranges of $Re < 40$ and $40 < Re < 300$, though both short and tall films have the same slopes of *Sh* at the both ranges. This may be attributed to the growth of the concentration boundary layer in the films. Miyara's [32] and Nagasaki et al.'s [33] numerical simulations of wavy film flow and diffusion

into the film showed that humps have gentle flow circulations in the near-peak regions of the humps, and the flow is rather *smooth laminar* (or not wavy) near the wall under the humps and in the substrate between humps. The hump-induced convections seem to cause partial renewals of the concentration boundary layer at and near the film surface [30], but the layer continuously grow in the near-wall region under humps and between humps, and therefore *Sh* decreases with increasing length of the developing boundary layer, i.e. the film height. The solutions to the diffusion equation in Nusselt film by Tamir and Taitel [34] are much smaller than the measurements of *Sh* for the wavy films at any *Re*, and the solution for the short film is larger than that for the tall film. The wave-induced convections dominate the interfacial mass transfer between the surface and the bulk [30] while the continuously developing boundary layer is limited to the near wall region and has small effects on the mass transfer. Thus, the measurements of *Sh* are larger for the short film than the tall film only by 17% in spite of the much larger differences in the *Sh* solution between the short and tall flat films.

The present measurements in *Sh* may have a fairly large error at the turbulent-flow range of *Re* though the error is small at the laminar-flow range. The number of bubbles entrained into the water pool greatly increases at the turbulent-flow range, and the bubble separator employed could not remove the bubbles completely. The gas absorption from the bubbles may increase the measurements of C_{out} and *Sh*, and cause deviations of the measurements from the Bakopoulos correlations at the turbulent-flow range (see Fig. 5). The excess absorption from the bubbles has a larger ratio to the absorption through the film surface for a shorter film causing a larger deviation. The deviation is approximately +18% and +34% for forced waves on 0.95 and 0.37 m tall films having negligible smooth entry passes, respectively, and the same amounts of deviation are observed for the natural waves at $Re > 700$ where the smooth entry pass disappears. The slope of *Sh*–*Re* curve is approximately 1.25 for forced waves on both 0.95 and 0.37 m tall films at $Re > 400$, and the slope itself is in good agreement with that of Bakopoulos' correlation. These observations may agree with Bakopoulos' measurements of *Sh* for 0.45 and 0.95 m tall films covered with natural waves. The 0.45 and 0.95 m tall films showed large deviations from his correlation for the turbulent-flow range, and the deviations are much larger than the present ones. The bubble separator installed in our apparatus seemed to reduce the deviation significantly.

In a similar manner to the abrupt increases of the heat and mass transfer observed in wall boundary shear layers, both the 0.37 and 0.95 m long films covered with natural waves show sharp rises in *Sh* at the transition range of $400 < Re < 700$ (Fig. 5). Associated with the smooth entry pass shortening rapidly the slope of *Sh* for natural waves is much larger at $400 < Re < 700$ than the 1.25 slope of Bakopoulos equation. The *Sh* for natural waves catches up with the values for forced waves and then increases with the 1.25 slope at $Re \sim 700$ or larger. This is more evident for the short film as shown in Fig. 5b. These sharp rises in *Sh* suggest that in the films with deceleration inlet flow, the laminar developing entry region is not longer than 0.37 m long tube at $Re \sim 400$, and it rapidly retracts upstream with increasing *Re* at the transition range of $400 < Re < 700$ in a similar manner to the smooth entry pass (Fig. 4). The developing entry region should be longer than the smooth entry pass since the waves with large surface-height fluctuations that trigger localized turbulences [21], develop downstream of the appearance of dimples. The transition starts at about 400 even in the 0.37 m film with decelerating inlet flow, which is much shorter than the 0.9–1.3 m long laminar developing entry region observed at $370 < Re < 750$ by Takahama and Kato [13]. Furthermore, the smooth entry pass rapidly shortens on the present films of the decelerating inlet flow with increasing *Re* at $400 < Re < 700$ (Fig. 4) while its length further stretch out and then levels out on films with the accelerating inlet flow (see Fig. 4 for Tailby and Portalski's [8] curve). These suggest that the decelerating inlet flow triggers the transition to turbulent flow at a further upstream location and makes the *Re* transition range narrower than the accelerating inlet flow.

The inlet forcings might account for a contraction in the transition range of *Re* to a nearly single, sharply defined critical value, and reduce the critical *Re* for the onset of turbulent flow from 400 to about 300. The measurements of *Sh* start to increase rapidly with a slope of 1.25 at $Re \sim 300$ for forced waves on both the tall and short films, shifting the second break from $Re = 400$ to 300 (Fig. 5). These support the *localized-turbulent flow* in film flow; the inlet forcings trigger the tall humps with long separations to develop shortly downstream of the inlet, and such tall humps may induce localized turbulences under the humps. A shift of the critical *Re* was also observed by Brauer [11]. He showed that a 0.3 mm diameter wire on the tube wall triggers the turbulent flow downstream in a film at $Re = 340$ or larger; otherwise the critical *Re* is 400.

The ratio in k_L between a wave-covered film and an entirely flat film may directly show the waves' mass transfer enhancement (Fig. 6). The solutions [34] of k_L to the diffusion equation for Nusselt film has been assumed to be the k_L for the flat film. For films covered entirely with forced waves, the ratio of k_L sharply increases with *Re* at $Re < 40$ and then the slope of the ratio curve rapidly decreases beyond $Re \sim 40$. The k_L ratio has a local maximum at $Re \sim 50$ and then gradually decreases to a local minimum at $Re \sim 300$, and then rapidly increases at the turbulent-flow range. The ratio is larger

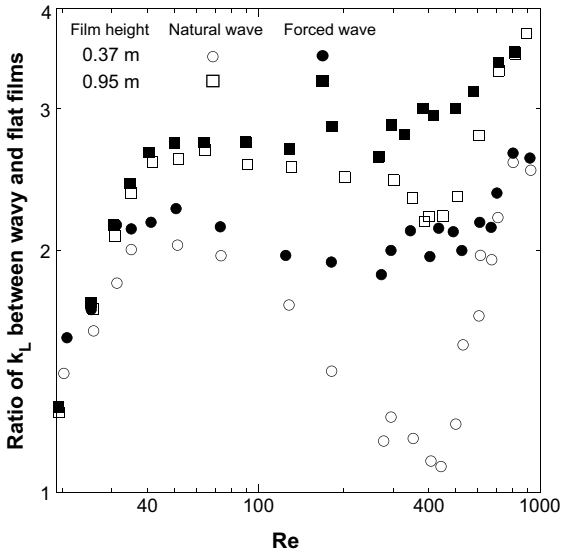

Fig. 6. Variation of mass transfer enhancement with Re for 0.95 and 0.37 m tall films covered with natural waves or forced waves. Ratios of k_L are presented between solutions [34] for flat film and measurements for wavy films.

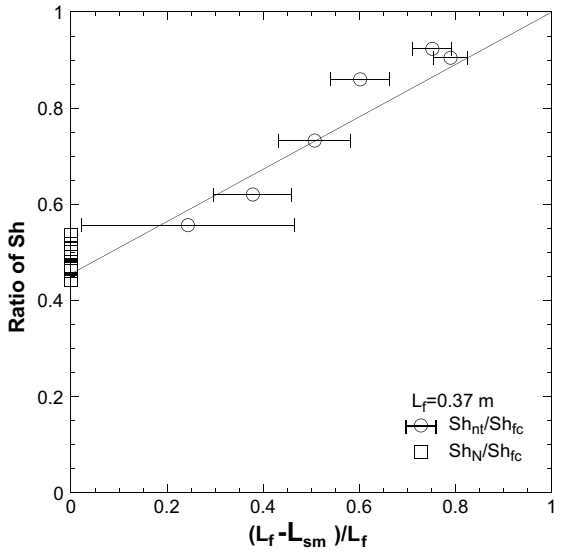

Fig. 7. Length $(L_f - L_{sm})$ of wavy region on film and variation of the ratio, Sh_{nt}/Sh_{fc}, between natural waves and forced waves for 0.37 m tall film at $40 < Re < 400$. The horizontal bars through plots represent the scattering in the length L_{sm} of the smooth entry pass (see Fig. 4), the fitting line is made by the method of least squares, and the ratio, Sh_N/Sh_{fc}, between solutions for smooth film and measurements for forced waves are plotted at vanishing $(L_f - L_{sm})$.

for the taller film, and the local maximum is approximately 2.7 and 2.2 for the tall and short films, respectively. The ratio is smaller for the natural waves than for the forced waves because of the smooth entry pass and the laminar developing entry region preceding the downstream region covered with natural waves, and the difference in the k_L ratio between the forced and natural waves is larger for the short film since the entry pass and the laminar region have larger fractions of their lengths to the film height on the short film. The ratio for the natural waves has the local minimum at $Re \sim 400$, and then sharply rises to catch up that for forced waves at $Re \sim 700$ or larger.

The deviation in Sh of natural waves from forced waves at the laminar-flow range (Fig. 5) is attributed largely to the smooth entry pass. The Sherwood number Sh_{nt} for natural waves with respect to Sh_{fc} for forced waves increases with the length $(L_f - L_{sm})$ of the wavy region downstream of the wave inception (Fig. 7), though the length scatters widely. The linear correlation fitting the plots is extrapolated to fall within the range of the solutions for the flat film Sh_N plotted at vanishing length $(L_f - L_{sm})$. At low Re of 40 around, the $(L_f - L_{sm})/L_f$ is large and the plots of Sh ratio are slightly larger than the linear correlation. At high Re close to 400, the $(L_f - L_{sm})$ is close to zero and the plots of Sh ratio are smaller than the correlation. These suggest that humps with less distorted wavefronts which appear at the low Re, enhance the mass transfer by a factor of larger number than humps with greatly distorted wavefronts accompanying dimples which appear at the high Re.

The 9.6 mm diameter of the present small tube may not have noticeable effect on the mass transfer. At the laminar flow range of Re, the present measurements are in good agreement with Bakopoulos [3] correlation (Fig. 5), and Bakopoulos constructed the correlations at laminar and turbulent flow ranges mainly from the data of Kamei and Oishi [5] for 47.6 mm inner diameter tube, Hikita et al. [4] for 27 mm inner diameter and Lamourelle and Shandall [6] for 16 mm outer diameter, respectively. Though our data have a 17% deviation from Bakopoulos correlation at the turbulent-flow range (Fig. 5a), such deviation should be attributed to the excess absorption from bubbles pulled into the water as described above, but not to the small diameter.

3.3. Effects of forcing frequency and tube inclination

The inlet forcings make the smooth entry pass to vanish and increase the mass transfer greatly in short films. For both 0.37 and 0.69 m tall films the amount of increase in the mass transfer changes with the frequency of the inlet forcings within small margins (Fig. 8). Yoshimura et al. [30] showed that humps triggered by the inlet forcings hold their wavefronts roughly horizontal at $Re < 55$ on a 0.24 m tall film and the mass

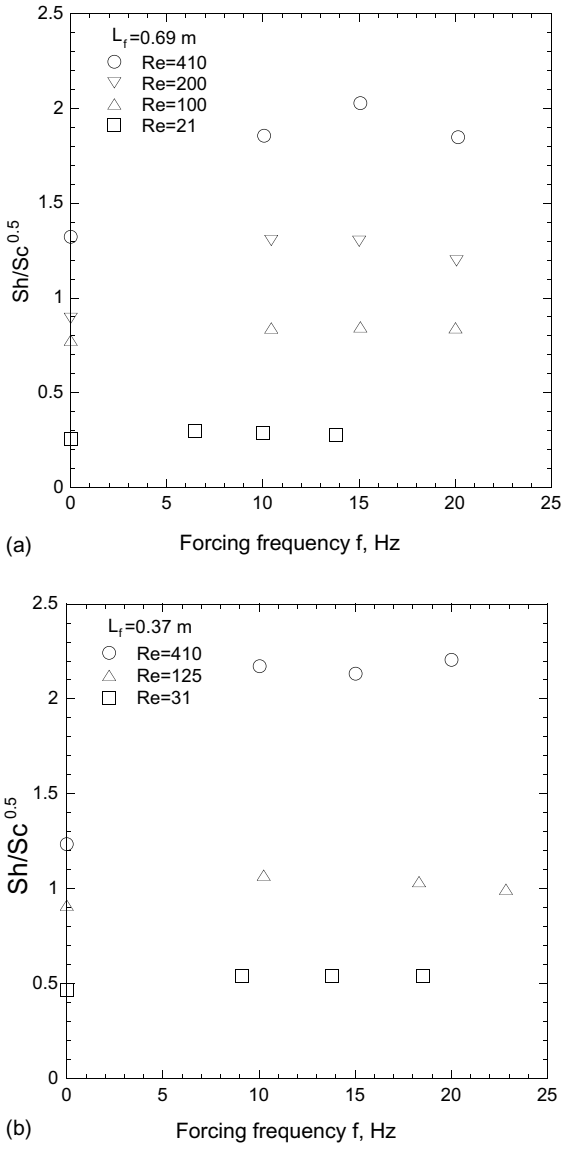

Fig. 8. *Sh* variations with forcing frequency f for (a) 0.69 m and (b) 0.37 m tall films.

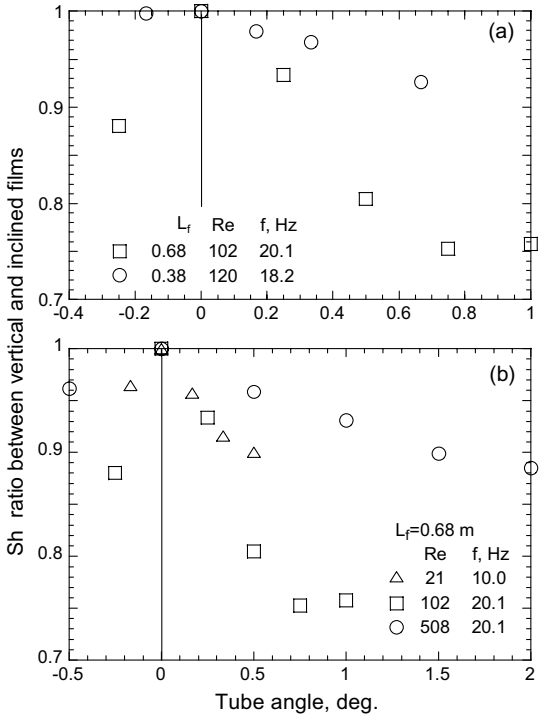

Fig. 9. Mass transfer reductions caused by tube inclination θ from the vertical: comparisons are presented (a) between 0.38 and 0.68 m tall films, and (b) between films of laminar and turbulent flow.

transfer enhancement by such two-dimensional humps changes with the forcing frequency within 15%. The forced waves were observed to critically increase the wavefront distortion at further downstream distances beyond $x = 0.24$ m at larger *Re* (see Fig. 2b and refer to [16]). The present results suggest that the frequency of such humps with distorted wavefronts changes the mass transfer enhancement within small margins.

A tube inclination from the vertical makes the hump wavefronts slant as they travel downstream (Fig. 3b). The partial disintegrations into dimples are fixed to the upper ends of the slanting wavefronts where the resulting dimples are released upstream, and dark strips representing hump wavefronts are observed more evidently. The wavefronts slant less rapidly at the turbulent-flow range of *Re* than the laminar-flow range (Fig. 3b). The *Sh* decreases with the tube inclination, and the decrease in *Sh* is more serious in the laminar-flow films than the turbulent-flow films, and is also true for taller films (Fig. 9). For a 0.68 m tall film, a 0.5° inclination causes decreases in *Sh* by 10–20% and by 4% in the laminar and turbulent flows, respectively.

4. Summary and discussion

In the film flow, the structure of turbulent flow and the transition from *wavy-laminar* to *turbulent* flow have not been fully understood. *Localized-turbulent flow* has been assumed by several researchers after Jackson [35]; turbulences are localized under large waves traveling on a thin substrate in which the flow is laminar otherwise. Recently Karimi and Kawaji [21,22] detected such localized turbulence under large waves at far downstream distances from the film inlet by rapid diffusion of laser-induced photochromic dye tracers. By the breaks appearing in curves of the mean film thickness vs. *Re*, Takahama and Kato [13] determined the laminar

developing entry region whose length decreases with increasing *Re* at the transition range. On the other hand, from measurements of the mass transfer, single critical Reynolds numbers have been determined by breaks in curves of the mean mass transfer coefficient k_L or *Sh* vs. *Re*, instead of *Re ranges* [3,5,7]. To our knowledge, the transition *range* of *Re* or the laminar developing entry region was first evidently captured on measurements of the mass transfer in the present work. Though the measurement error in *Sh* is fairly large at the transition and turbulent-flow ranges, the comparisons of the *Sh*–*Re* curve between natural waves and forced waves and between the tall and short films evidently showed the sharp rises in *Sh* at the transition range of *Re*, suggesting that the laminar developing entry region rapidly shortens at the transition range. Comparison of the present results with Takahama and Kato's [13] indicates that the length of the laminar developing region and the transition range of *Re* are sensitive to the inlet flow conditions.

For practical applications of the interfacial mass transfer processes, low flow rates of $40 < Re < 100$ are recommended in falling water films, at which the maximum mass transfer enhancement or near-maximum enhancement is available with low pumping power (Fig. 6), though Roberts and Chang [2] recommended the flow rates of $Re \sim 40$ based on their theoretical model analysis. To achieve uniform distribution at such low flow rates, the authors recommend the use of the feeding device employed in this work or one similar to it, i.e. 'undulated annular distributor' used by Brauer [19] and Bakopoulos [3]. Tubes should be aligned to be strictly vertical; otherwise for 0.7 m or taller films, a 0.2° inclination may cause 5% or larger reductions in mass transfer coefficient (Fig. 9). The inlet forcings are most effective when these are applied to short films at $150 < Re < 600$ where the smooth entry pass and the laminar developing entry region have large fractions of their lengths to the film height. The forcings drastically shorten the smooth entry pass and the laminar developing region to enhance the mass transfer, though the enhancement changes with the frequency of the forcings within small margins.

Acknowledgements

The authors gratefully acknowledge S. Ohkawa and T. Shimada for their assistance in the experimental work. This work was supported by Japan Society for the Promotion of Science.

References

[1] S.V. Alekseenko, V.E. Nakoryakov, B.G. Pokusaev, Wave Flow of Liquid Films, Begell House Inc., New York, 1994.
[2] R.M. Roberts, H.-C. Chang, Wave enhanced interfacial transfer, Chem. Eng. Sci. 55 (2000) 1127–1141.
[3] A. Bakopoulos, Liquid-side controlled mass transfer in wetted-wall tubes, Ger. Chem. Eng. 3 (1980) 241–252.
[4] H. Hikita, K. Nakanishi, T. Kataoka, Chem. Eng. (Jpn.) 23 (1959) 459–466.
[5] S. Kamei, J. Oishi, Mass and heat transfer in a falling liquid film of wetted wall tower, Mem. Faculty Eng., Kyoto Univ. 17 (4) (1955) 277–284.
[6] A.P. Lamourelle, O.C. Sandall, Gas absorption into a turbulent liquid, Chem. Eng. Sci. 27 (1972) 1035–1043.
[7] R.E. Emmert, R.L. Pigford, A study of gas absorption in falling liquid films, Chem. Eng. Prog. 50 (1954) 87–93.
[8] S.R. Tailby, S. Portalski, Wave inception on a liquid film flowing down a hydrodynamically smooth plate, Chem. Eng. Sci. 17 (1962) 283–290.
[9] G.D. Fulford, The flow of liquids in thin films, in: Advances in Chemical Engineering, vol. 5, Academic Press, New York, 1964, pp. 151–236.
[10] S. Portalski, A.J. Clegg, An experimental study of wave inception on falling liquid films, Chem. Eng. Sci. 27 (1972) 1257–1265.
[11] H. Brauer, Stromung and Warmeubergang bei Rieselfilmen, VDI (Ver. Deut. Ingr.)-Forschungshelt, 1956, p. 457.
[12] D.R. Webb, G.F. Hewitt, Downwards co-current annular flow, Int. J. Multiphase Flow 2 (1975) 35–49.
[13] H. Takahama, S. Kato, Longitudinal flow characteristics of vertically falling liquid films without concurrent gas flow, Int. J. Multiphase Flow 6 (1980) 203–215.
[14] R.P. Salazar, E. Marschall, Time-average local thickness measurement in falling liquid film flow, Int. J. Multiphase Flow 4 (1978) 405–412.
[15] T.D. Karapantsios, A.J. Karabelas, Longitudinal characteristics of wavy falling films, Int. J. Multiphase Flow 21 (1) (1995) 119–127.
[16] C.D. Park, T. Nosoko, Three-dimensional wave dynamics on a falling film and associated mass transfer, AIChE J. 49 (11) (2003).
[17] K.J. Chu, A.E. Dukler, Statistical characteristics of thin, wavy films, Part III. Structure of the large waves and their resistance to gas flow, AIChE J. 21 (1975) 583–593.
[18] H.-C. Chang, E.A. Demekhin, E. Kalaidin, Simulation of noise-driven wave dynamics on a falling film, AIChE J. 42 (1996) 1553–1568.
[19] H.-C. Chang, E.A. Demekhin, E. Kalaidin, Y. Ye, Coarsening dynamics of falling-film solitary waves, Phys. Rev. E 54 (1996) 1467–1477.
[20] H.-C. Chang, E.A. Demekhin, S.S. Saprikin, Noise-driven wave transitions on a vertically falling film, J. Fluid Mech. 462 (2002) 255–283.
[21] G. Karimi, M. Kawaji, An experimental study of freely falling films in a vertical tube, Chem. Eng. Sci. 53 (1998) 3501–3512.
[22] G. Karimi, M. Kawaji, Flow characteristics and circulatory motion in wavy falling films with and without countercurrent gas flow, Int. J. Multiphase Flow 25 (1999) 1305–1319.
[23] K. Feind, Strömungsuntersuchungen bei Gegenstrom von Rieselfilmen und gas in lotrechten Rohren, VDI-Forschungsheft, 1960, p. 481.

[24] W. Wilke, Wärmeübergang an Rieselfilme, VDI (Ver. Deut. Ingr.)-Forschungshelt, 1962, p. 490.
[25] H. Brauer, H. Thiele, Chem. -Anlagent Verfahren 4 (1975) 28–30 (reported in Ref. [3]).
[26] W. Malewski, Chem. -Ing. -Tech. 40 (1968) 201–206 (reported in Ref. [3]).
[27] F.W. Pierson, S. Whitaker, Some theoretical and experimental observations of the wave structure of falling liquid films, Ind. Eng. Chem., Fundam. 16 (4) (1977) 401–408.
[28] G.A. Truesdale, A.L. Downing, G.F. Lowdan, The solubility of oxygen in pure water and sea-water, J. Appl. Chem. 5 (1955) 53–62.
[29] T. Nosoko, P.N. Yoshimura, T. Nagata, K. Oyakawa, Characteristics of two-dimensional waves on a falling liquid films, Chem. Eng. Sci. 51 (1996) 725–732.
[30] P.N. Yoshimura, T. Nosoko, T. Nagata, Enhancement of mass transfer into a falling laminar liquid film by two-dimensional surface waves (some experimental observations and modeling), Chem. Eng. Sci. 51 (1996) 1231–1240.
[31] F.P. Stainthorp, J.M. Allen, The development of ripples on the surface of a liquid film flowing inside a vertical tube, Trans. Inst. Chem. Eng. 43 (1965) T85–T91.
[32] A. Miyara, Numerical simulation of wavy liquid film flowing down on a vertical wall and an inclined wall, Int. J. Thermal Sci. 39 (2000) 1015–1027.
[33] T. Nagasaki, H. Akiyama, H. Nakagawa, Numerical analysis of flow and mass transfer in a falling liquid film with interfacial waves, Thermal Sci. Eng. 10 (2002) 17–23.
[34] A. Tamir, Y. Taitel, Diffusion to flow down an incline with surface resistance, Chem. Eng. Sci. 26 (1971) 799–808.
[35] L.J. Jackson, Liquid films in viscous flow, AIChE J. 1 (1955) 231–240.